Journal of Hazardous Materials 186 (2011) 76–83

Contents lists available at ScienceDirect

Journal of Hazardous Materials

journal homepage: www.elsevier.com/locate/jhazmat

Adsorption behavior of phosphate on lanthanum(III)-coordinated diamino-functionalized 3D hybrid mesoporous silicates material

Jianda Zhang[a,b], Zhemin Shen[a,*], Wenpo Shan[c], Zhijian Mei[a], Wenhua Wang[a]

[a] School of Environmental Science and Engineering, Shanghai Jiaotong University, 800#, Dongchuan Road, Shanghai 200240, PR China
[b] Tianjin Hydraulic Research Institute, 60#, Youyi Road, Tianjin 300000, PR China
[c] College of Chemistry and Environmental Science, Hebei University, Baoding 071002, PR China

ARTICLE INFO

Article history:
Received 25 February 2010
Received in revised form 18 October 2010
Accepted 19 October 2010
Available online 27 October 2010

Keywords:
MCM-41
Lanthanum
Phosphate
Adsorption

ABSTRACT

An inorganic/organic hybrid adsorbent for phosphate adsorption was synthesized by introducing lanthanum (La) onto diamino modified MCM-41. The adsorbent was characterized by XRD, SEM, BET, TGA, and FTIR spectroscopy. A series of batch tests were conducted to investigate the influence of contact time, initial phosphate concentration, pH of the solution, and competitive ions on the phosphate adsorption capacity. The Langmuir and Freundlich models were used to simulate the sorption equilibrium, and the results indicated that the Langmuir model fitted the experiment data better than the Freundlich model. The maximum adsorption capacity calculated from the Langmuir model is 54.3 mg/g. For kinetic study, phosphate adsorption followed the pseudo-second-order equation well with a correlation coefficient greater than 0.99. Optimum pH value for the removal of phosphate was between 3.0 and 7.0. The presence of Cl^- and NO_3^- has neglectable influence on the phosphate adsorption. F^- and SO_4^{2-} have negative effects on the adsorption of phosphate. Phosphate on the spent adsorbent can be almost released by 0.01 M NaOH solution in 12 min.

1. Introduction

Phosphate is considered to be one of the key nutrient elements for the growth of biological organisms in the aquatic environments. However, an excess of phosphate present in water often induces eutrophication [1,2], which leads to the overgrowth of the phytoplankton, causing oxygen lack, water quality reduction and aquatic animal depopulations. Furthermore, some algal blooms are toxic to plants and animals. For example, freshwater algal blooms can pose a threat to livestock because the algae can release some neuro and hepatotoxins when they are eaten by the lives. Furthermore, the toxins may threaten the human health following the food chain [3,4]. The well known event of Lake Tai' water bloom was attributed to the eutrophication caused by the excess of the nutrient in the lake [5].

To avoid eutrophication occurring, it is necessary to control the phosphate concentration in water bodies. Recently, various wastewater treatment technologies, including physicochemical precipitation, advanced biological treatment and physical method, have been applied to remove the phosphate. Among them, removal of phosphate through adsorption becomes the focus because it is convenient and cost-effective. The adsorbents can be divided into inorganic materials, organic materials and silica-based mesoporous inorganic/organic hybrid materials. The inorganic adsorbents include alum and aluminum hydroxide [6], calcium kaolinite [7], layered double hydroxides [8], calcite [9], zeolite [10], dolomite [11], red mud [12], fly ash [13] and blast furnace slag [14]. The organic materials, especially biomaterials contain collagen fiber [15], shell powder [16], bark [17], wood particle [18], banana stem [19] and orange waste [20]. Silica-based mesoporous inorganic/organic hybrid materials [21,22] are a new type of material characterized by large specific surface areas and pore size (2–15 nm), which are obtained through the coupling of inorganic and organic components by postsynthesis. Besides adsorption, the incorporation of functionalities enables the materials to be used in lots of other fields such as catalysis, chromatography, molecular switches and the construction of systems for controlling the release of active compounds [23–26].

MCM-41 which is a member of the family of mesoporous molecular sieve has a self-assembled molecular array with surfactant molecules as a structure directing template [27]. The high density of silanol groups on the pore wall is favorable for the introduction of functional groups with high coverage [28]. Fryxell synthesized copper-coordinated, ethylenediamine modified mesoporous silicate as an anion adsorbent and this adsorbent has 3-fold symmetry structure which can match the geometry of tetrahedral anions [29].

* Corresponding author at: School of Environmental Science and Engineering Shanghai Jiaotong University, 800 # Dongchuan Road, Shanghai 200240, PR China. Tel.: +86 21 54745262; fax: +86 21 54745262.
E-mail addresses: zmshen@sjtu.edu.cn, zheminshenxs@163.com (Z. Shen).

0304-3894/$ – see front matter © 2010 Elsevier B.V. All rights reserved.
doi:10.1016/j.jhazmat.2010.10.076

Recently, Lanthanum has been used to remove phosphate from water solutions. Shin et al. [17] had introduced lanthanum as an inorganic material into bark fiber to develop an adsorbent for phosphate capture. Wu et al. [30] had bound lanthanum to chelex-100 resin and found that the La–chelex resin was able to remove phosphate efficiently. In conclusion, lanthanum has the potential to synthesize efficient adsorbent for phosphate adsorption.

In this study, a new inorganic/organic hybrid adsorbent for phosphate adsorption was synthesized by introducing lanthanum (La) onto diamino modified MCM-41. The new adsorbent was denoted as La-NN-M41. We focused on the preparation as well as the characterization of the adsorbent La-NN-M41 and its fundamental adsorption behavior of removing phosphate from aqueous solutions, including the adsorption kinetics, adsorption isotherm, and the effect of pH. Desorption kinetic was performed under NaOH solution (0.01 M). Effects of foreign anions in aqueous solution, such as F^-, Cl^-, $NO_3{}^-$, $SO_4{}^{2-}$ have also been investigated.

2. Materials and methods

2.1. Preparation of materials

MCM-41 was synthesized following the procedure described elsewhere with a templating method. Tetraethylorthosilicate (TEOS) was used as organic Si source and cetyltrimethylammonium bromide (CTAB) as template [31]. 4.89 g CTAB was added to the mixture of 40 g distilled water and 2.15 g NaOH. After that, 5 mL TEOS was added slowly to the mixture until the solution became a clear gel. Then it was stirred for 2 h and transferred into PTFE-lined autoclaves under autogenous pressure at 110 °C for a period of 48 h. The white solid product was washed, filtered, dried, and calcined at 550 °C with the heat rate of 1 °C min^{-1}.

The amino-functionalized MCM-41 was prepared via the postsynthesis grafting method according to Yokoi et al. [32]. 5 g calcined MCM-41 was stirred vigorously in dry toluene with 15 mL 1-(2-aminoethyl)-3-aminopropyltrimethxoysilane, $H_2NCH_2CH_2NHCH_2CH_2CH_2Si(OCH_3)_3$ (Momentive Performance Materials Inc.). The mixture was heated at 110 °C under inert atmosphere for 6 h. The functionalized material was purified by filtration, washed with 2-propanol, and dried at 100 °C. The powder was denoted as NN-M41.

Excess amount of La(III) nitrate hexahydrate in 2-propanol solution with NN-M41 were stirred for 2 h at 25 °C. The powder was collected by filtration, washed by 2-propanol and dried at 110 °C. The product was denoted as La-NN-M41.

2.2. Characterization of materials

Surface morphologies of MCM-41 and La-NN-M41 samples were examined by scanning electron microscopy (JSM-7401F, JEOL Ltd., Japan). Before that, the samples were dried at 120 °C for 12 h. X-ray powder diffraction patters of the prepared samples were recorded in the 2θ range of 0.8–8° with a scan speed of 1°/min by using a diffractometer (D/max-2200/PC, Rigaku Corporation, Japan) with Cu Kα radiation (40 mA, 45 kV). The pore structures distribution and BET specific area of the samples were measured by N_2 adsorption/desorption technique on Surface Area and Porosimetry Analyzer (ASAP 2010 M+C, Micromeritics Inc., USA). Prior to analysis, the pure MCM-41 was degassed at 200 °C for 6 h under vacuum, and functionalized materials were degassed at 120 °C for 12 h under vacuum. Fourier transform infrared (FTIR) measurements of each sample were performed between 200 and 4000 cm^{-1} by using Shimadzu IRPrestige-21 instrument with 2 cm^{-1} resolution to check the changes of the functional groups of the samples. KBr pellets containing 0.5% of the samples were used in FTIR experiment. Thermogravimetric analyses (TGA) were performed with TGA 7 system (Perkin Elmer, Inc., USA) to determine the amount of organsilane moieties present on La-NN-M41. The CN elemental analysis was determined by elemental analyzer (Vario EL III, Elementar Corporation, USA). The organic group content of the functionalized mesoporous silica was calculated based on the nitrogen content.

2.3. Phosphate adsorption experiments

As for the equilibrium experiments, 0.100 g adsorbent was added to 250 mL glass-stoppered conical flasks with 100 mL phosphate solution with various initial concentrations. The phosphate solution was prepared by using anhydrous K_2HPO_4 and deionized water. The initial pH of the phosphate solution was adjusted to 6.0 with 1 mol/L NaOH and HCl. The total volume added for pH adjustment never exceeded by 1% pH values using pH meter combined with glass electrode (pHS-3TC, Shanghai Hongyi Instrument Factory, Shanghai, China). The conical flasks were transferred into Air Bath Thermostatic Rotary Shaker (HZQ-F, Harbin Donglian Electronic & Technology Development Co. Ltd.) at various temperatures (25, 35 and 45°C), shaken at 120 rpm. At the end of adsorption process, the supernatant was filtered through 0.45 μm membrane syringe filter and analyzed by using ascorbic acid method to monitor the absorbance at 880 nm with spectrophotometer (UV-2102 PCS, Unico Corp, China) [33]. The amount of phosphate adsorbed on La-NN-M41 at equilibrium was calculated by

$$q_e = \frac{(C_o - C_e)V}{m} \quad (1)$$

where C_o and C_e (mg/L) are the initial and equilibrium liquid phase phosphate concentrations, respectively, V (L) is the volume of the solution and m (g) is the mass of the adsorbent.

Adsorption kinetic experiments were conducted as follows: 0.100 g adsorbent was added in 100 mL phosphate solution, and the initial concentration of phosphate solution was 30, 50, 100 mg/L, respectively. The pH was adjusted to 7.0 by using the same method in equilibrium experiments. The sealed flasks were then placed in shaker bath at 25 °C, shaken at 120 rpm. The suspension solution was taken out of flasks at determined time intervals for the analysis of phosphate concentration.

To investigate the influence of pH on phosphate adsorption, the experiments were conducted at various initial pH, ranging from 2.0 to 12.0. 50 mg/L phosphate solution and 1.00 g adsorbent per liter of solution were used in the experiments.

Besides the influence of pH, the effect of coexisting anions on phosphate adsorption was evaluated. Various concentrations (100, 300, 500, 700, 900 mg/L) of sodium salt form of coexisting anions such as F^-, Cl^-, $NO_3{}^-$, $SO_4{}^{2-}$ were added into phosphate solution. Initial phosphate concentration of 50 mg/L and 1.00 g adsorbent per liter of solution were used in the experiments. The initial pH of final solution was adjusted to 6.0.

2.4. Desorption kinetic study

Desorption kinetic study was carried out to investigate the feasibility of the spent adsorbent's reuse. The phosphate loaded adsorbent was filtered from the mixture by using 0.45 μm syringe filter and washed carefully with deionized water to remove any unabsorbed phosphate. Then the spent adsorbent was mixed with 100 mL 0.01 M NaOH solution, the samples were taken out at interval time and the desorbed phosphate was estimated.

3. Results and discussion

3.1. X-ray diffraction

The X-ray diffraction patterns of MCM-41, NN-M41, and La-NN-M41 are presented in Fig. 1. Well-resolved peaks of MCM-41 were

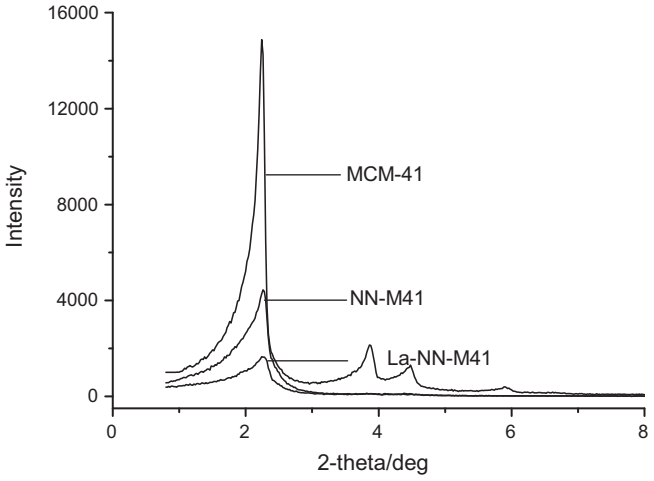

Fig. 1. X-ray diffraction patterns of MCM-41, NN-M41 and La-NN-M41.

displayed in the (1 0 0), (1 1 0), and (2 0 0) planes, which indicates the typical hexagonal long-range arrays structure of mesoporous material [34]. From the XRD pattern and SEM images (Fig. 1), some discernible differences could be found in the textural properties between MCM-41 and La-NN-M41. The edge of the MCM-41 particle is sharper than La-NN-M41's, which is mainly caused by grafting organoalkoxysilanes. Compared to the XRD patterns of MCM-41, the decrease of peak (1 0 0) reflection intensity could be observed for NN-M41 and La-NN-M41, and the peak of NN-M41 was higher than that of La-NN-41's. After postsynthesis grafting, the reduction in the (1 0 0) peaks intensity and disappearance of (1 1 0) and (2 1 0) peaks of the modified samples may be attributed to the partial collapse of the hexagonal long-range arrays structure, which can be considered resulting from poor hydrothermal stability of the material and flexibility of the siliceous framework produced by the stress of anchored La metal complex [35,36].

3.2. Nitrogen adsorption and desorption

The nitrogen adsorption–desorption isotherms of MCM-41, NN-M41 and La-NN-M41 are shown in Fig. 2. All the nitrogen adsorption–desorption isotherm represented typical type IV model according to International Union of Pure and Applied Chemistry Classification and the pure MCM-41 has H1 hysteresis loop which was representative of mesopores [37]. The NN-M41 and La-NN-M41 samples showed an isotherm with adsorption step shifting toward lower relative pressures. The nitrogen adsorption experiments results (BET specific surface area, pore diameter and pore volume) are summarized in Table 1. The BET specific surface areas of MCM-41, NN-M41 and La-NN-M41 are 1015, 348 and 134 m^2/g, respectively. The corresponding pore diameters are 2.87, 2.82 and 2.61 nm respectively. The pore volumes are 0.89, 0.19 and 0.10 cm^3/g, respectively. The change trend is attributed to the grafted silane and the La^{3+} complexation. Such phenomena are usually observed after post-grafting procedure [38].

Table 1
Structure characteristics of MCM-41, NN-M41 and La-NN-M41.

Samples	BET surface area (m^2/g)	Pore diameter (nm)	Total pore volume (cm^3/g)
MCM-41	1015	2.87	0.89
NN-M41	348	2.82	0.19
La-NN-M41	134	2.61	0.10

3.3. FTIR and TGA analysis

The FTIR, which was used to characterize the surface silanols and hydrogen-bonded hydroxyl groups is shown in Fig. 3. The bands at 1080, 808, and 975 cm^{-1} corresponded to the Si–O–Si asymmetric and symmetric vibrations. The broad band (3600–3200 cm^{-1}) in the hydroxyl region could be seen to illustrate the presence of silanol groups within the MCM-41 pore channel. After grafting the diamino-organic moiety, the bands at 2944 cm^{-1} which indicates the C–H stretching vibration could be observed. The weak bands at 1470 and 1658 cm^{-1} are due to NH_2 vibrations. These results confirmed that the diamino species were anchored on the surface of MCM-41. After immobilization of the La^{3+}, the amine bands shifted to lower wavenumber suggesting the possibility of the La^{3+} anchored on the active sites. $La(NO_3)_3$ was used as La source, and the peak at the 1384 cm^{-1} was due to the introduction of nitrate. TGA analysis was used to evaluate the amount of silanes and weakly adsorbed water in the adsorbent. For the MCM-41 sample (Fig. 4), the slight weight loss was caused by the loss of weakly physisorbed water in the pore of the sample. The TGA spectrum of La-NN-M41 showed a sharp weight loss between 200 and 600 °C. That is because the diamino-organic groups and the siloxane groups on the surface decomposed. The elemental analysis results showed that the C and N content was 13.21% and 5.01%, which well matched the molecular formula of diamino groups $C_5N_2H_{13}$. We measured the content of La in adsorbent by ICP, and the content of La is 8.6%. In view of the

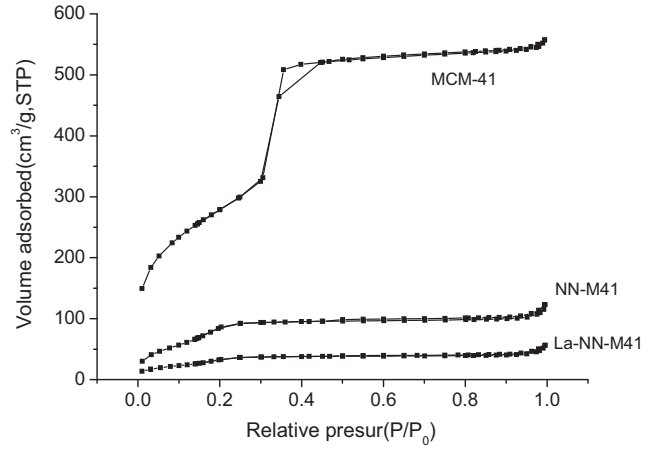

Fig. 2. Nitrogen adsorption–desorption isotherms of MCM-41, NN-M41 and La-NN-M41.

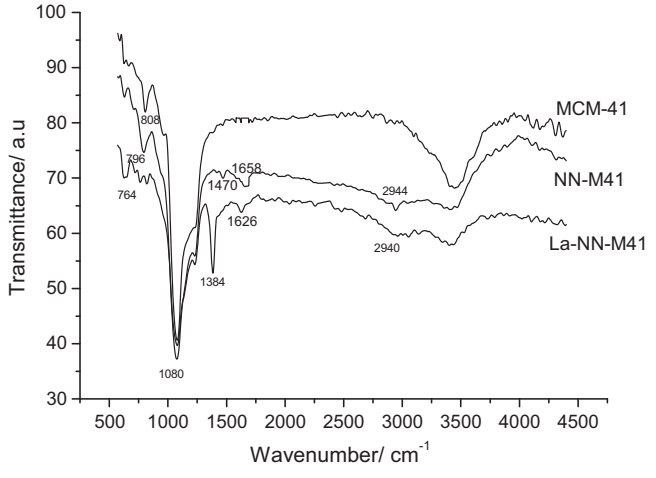

Fig. 3. IR spectra of each samples: (a) MCM-41, (b) NN-MCM-41 and (c) La-NN-MCM-41.

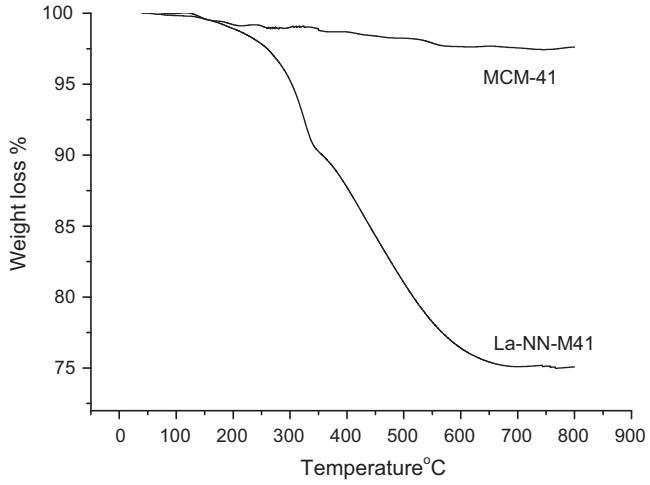

Fig. 4. Thermal gravimetric analyses data of samples.

Table 2
Estimated Langmuir and Freundlich isotherms parameters for phosphate adsorption.

Temperature	Langmuir			Freundlich		
(°C)	q_0 (mg/g)	K_L (L/mg)	R^2	n	K_F (mg/g)	R^2
25	54.3	0.065	0.995	11.3	32.4	0.956
35	51.8	0.092	0.996	7.9	24.8	0.927
45	50.3	0.138	0.997	6.6	20.6	0.928

above results, it can be proved that the organosiloxane groups were linked to the MCM-41 surface by postsynthesis grafting reaction.

3.4. Adsorption isotherms

Phosphate adsorption isotherms on La-NN-M41 were obtained at different temperatures (25, 35, and 45 °C) by varying the initial phosphate concentration. The isotherms data were fitted to well-known Langmuir and Freundlich isotherms models presented in Eqs. (2) and (3) by non-linear regression with the method of the least squares.

The Langmuir model which is valid for monolayer adsorption onto surface with a finite number of identical sites is expressed as

$$\frac{C_e}{q_e} = \frac{1}{q_0 K_L} + \frac{C_e}{q_0} \quad (2)$$

where C_e (mg/L) is the concentration of phosphate solution at equilibrium, q_e (mg/g) is the corresponding adsorption capacity. q_0 (mg/g) and K_L (L/mg) are Langmuir constants related to adsorption capacity (mg/g) and energy or net enthalpy of adsorption, respectively.

The logarithmic form of Freundlich model is expressed as

$$\log q_e = \log K_F + \frac{1}{n}\log C_e \quad (3)$$

where q_e (mg/g) is the corresponding adsorption capacity, C_e (mg/L) is the concentration of phosphate solution at equilibrium. K_F (mg/g) and n are the constants.

The Langmuir and Freundlich model's fitting curves are shown in Fig. 5. The estimated adsorption constants with correlation coefficient obtained from the isotherm are listed in Table 2. It is seen that both Langmuir and Freundlich equation can satisfactorily describe the isotherms experimental data ($R^2 > 0.9$). However, in terms of R^2 values, the Langmuir equation is more suitable than Freundlich equation in describing the adsorption isotherms. In previous study, researchers reported that the phosphate adsorption on many adsorbent fit the Langmuir equation. Li et al. [39] presented that the phosphate adsorption on lanthanum doped vesuvianite was better fitted by the Langmuir equation than the Freundlich equation did. The isotherm of phosphate onto La-load orange waste [20] and La-modified bentonite [40] also well followed the Langmuir equation. For Langmuir equation, the value of q_0 decreases from 54.3 mg/g to 50.3 mg/g with the increase of temperature, which exhibits the exothermic nature of the adsorption process. Table 3 presents the comparison of adsorption capacity of La-NN-M41 with other adsorbent for phosphate adsorption. Since the adsorption was under different experimental conditions, the adsorption capacity of the adsorbents is not strictly comparable. In general, La-NN-M41 exhibits higher adsorption capacity than certain adsorbents, but lower than that of activated alumina and Al impregnated SBA-15.

3.5. Adsorption kinetics studies

Kinetic studies were carried out to determine the rate of phosphate removal from solution by La-NN-M41. The initial phosphate concentrations were 30, 50, 100 mg/L, respectively. Fig. 6 shows the change of adsorption capacity as a function of initial phosphate concentration and contact time. The adsorption process reached to equilibrium in less than 60 min in the three kinetic studies. The maximum phosphate adsorption capacity is found to be 31.9, 42.4, and 44.7 mg/g, respectively with different initial concentrations at 25 °C. From Fig. 6, it is clear that when the initial phosphate con-

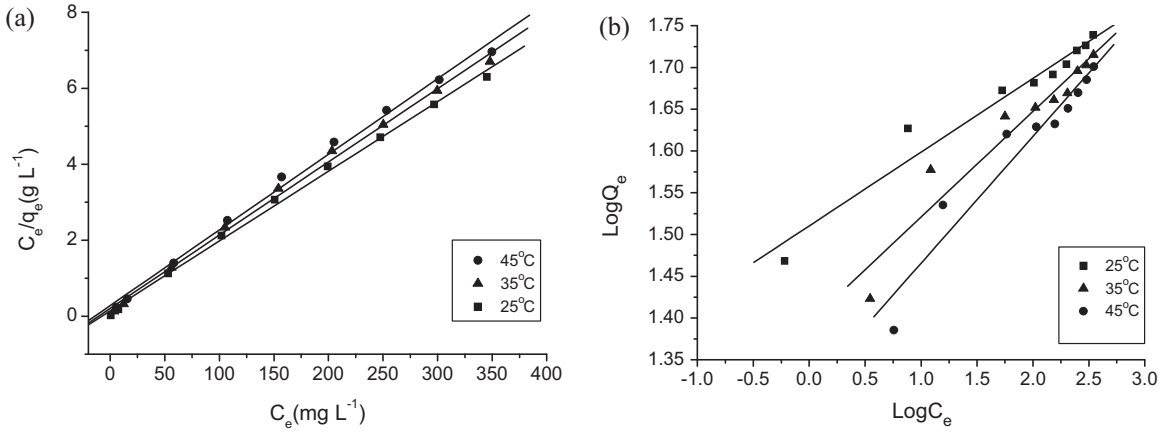

Fig. 5. (a) Linear Langmuir adsorption isotherms at 25, 35 and 45 °C and (b) Freundlich adsorption isotherms at 25, 35 and 45 °C.

Table 3
Comparison of phosphate adsorption capacities of various adsorbents.

Adsorbent	pH	Temperature (°C)	Adsorption capacity (mg/g)	Data source
La-modified zeolite	6.0	20	24.6	[44]
La doped vesuvianite	7.1	–	20.5	[39]
Activated alumina	6.4	25	53.7	[45]
Al impregnated SBA-15	6.4	25	81.9	[45]
Fe–Mn binary oxide	5.6	25	36	[46]
MCM-48-NH_2-G	–	25	27.1	[38]
Mesoporous ZrO_2	6.7–6.9	25	29.7	[47]
La-NN-M41	7.0	25	54.3	Present work

Table 4
Comparison of the first- and second-order adsorption rate constants and experimental values for different initial phosphate concentrations.

Initial concentration C_0 (mg/L)	q_e (exp) (mg/g)	First-order kinetics			Second-order kinetics		
		k_1 (min^{-1})	q_e (cal) (mg/g)	R^2	k_2 (g/(mg min))	q_e (cal) (mg/g)	R^2
30	31.9	0.0400	3.2	0.612	0.0098	32.2	0.999
50	42.4	0.0297	16.2	0.862	0.0115	42.7	0.999
100	44.7	0.0184	10.5	0.577	0.0131	44.6	0.999

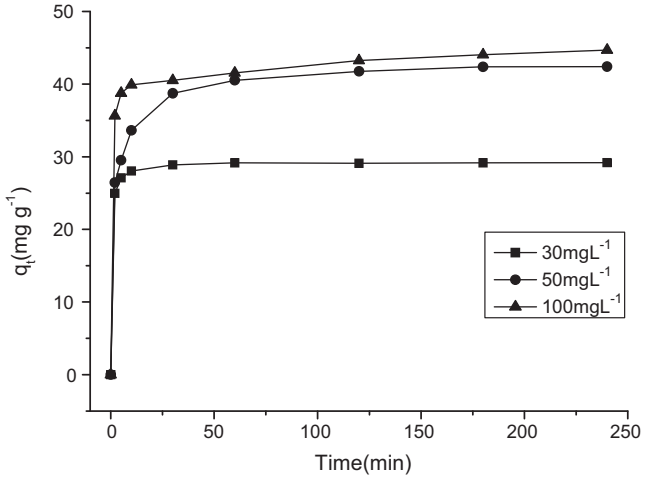

Fig. 6. Effect of agitation time and initial concentration of the amount of adsorption of phosphate onto La-NN-M41. adsorbent dose, 100 mg/100 ml; temperature, 25°C.

centration is mg/L, the adsorption process can be divided to three steps. In the first 5 min, the adsorption capacity increased fast and achieved 92.8% of the equilibrium adsorption capacity. That may be due to the large concentration gradient between bulk solution and adsorbent surface. In the following 55 min, the adsorption slowed down possibly resulted from more sorption sites being occupied. After 60 min, the adsorption reached equilibrium and the adsorption capacity did not change. Besides the adsorption capacities are higher, the adsorption process under 50 and 100 mg/L are similar to that under the 30 mg/L. In order to analyze the kinetic mechanism of the adsorption process, the kinetic data were fitted by pseudo-first-order model and pseudo-second-order model (Table 4). The pseudo-first-order equation is given as [41]:

$$\log(q_e - q_t) = \frac{\log q_e - k_1 t}{2.303} \quad (4)$$

where q_e (mg/g) and q_t (mg/g) are the amount of phosphate adsorbed at equilibrium and at time t (min), respectively, and k_1 is the adsorption rate constant of pseudo-first-order adsorption (1/min).

The second-order kinetics model [42] can be represented as

$$\frac{t}{q_t} = \frac{1}{k_2 q_e{}^2} + \frac{t}{q_e} \quad (5)$$

where k_2 is the equilibrium rate constant of pseudo-second-order adsorption (g/mg/min). Values of k_2 and q_e are calculated from the plot of t/q_e vs t.

The kinetic data fitted by pseudo-first-order and pseudo-second-order models are shown in Fig. 7 and the values of different parameters as well as corresponding correlation coefficients determined by both kinetic models for phosphate are shown in Table 2. In terms of correlation coefficients values, the pseudo-second-order kinetic model fitted better than pseudo-first-order kinetic model,

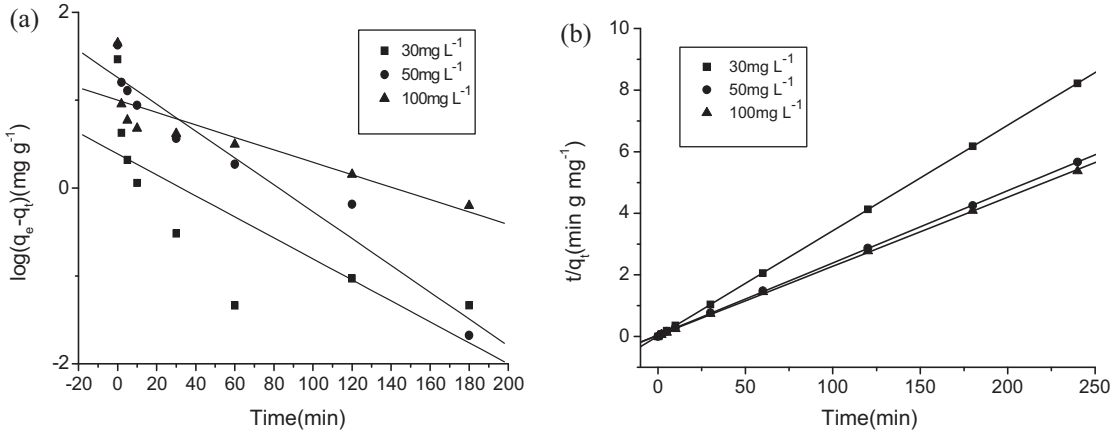

Fig. 7. (a) Peseudo-first-order plots for adsorption of phosphate on the adsorbent and (b) peseudo-second-order plots for adsorption of phosphate on the adsorbent.

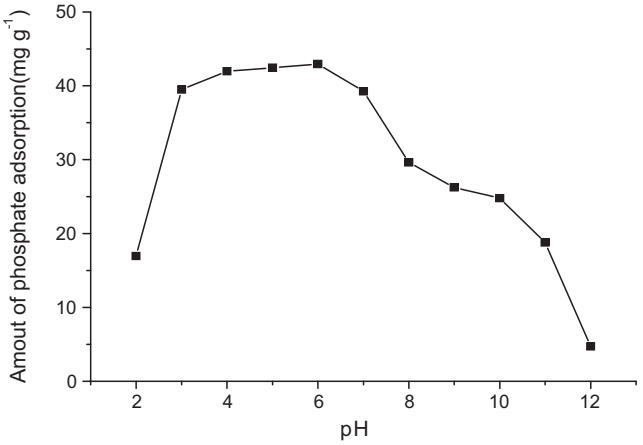

Fig. 8. Effect of pH on adsorption of phosphate: adsorption dose, 100 mg/100 ml; agitation time, 2 h; temperature, 25 °C.

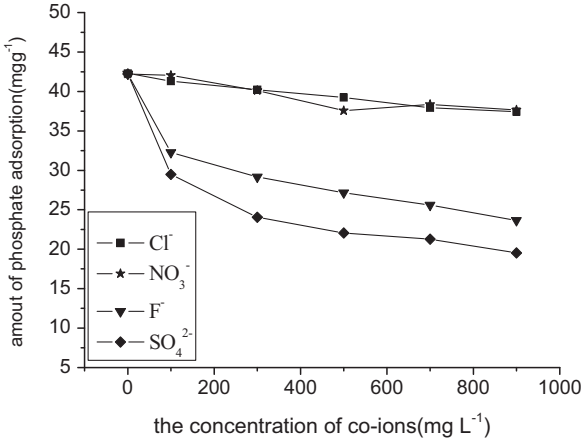

Fig. 9. Effect of co-ions on the phosphate adsorption.

which suggested that the adsorption process might be chemisorption.

3.6. Effect of initial pH on adsorption of phosphate

The effect of pH on the phosphate adsorption capacity of La-NN-M41 was investigated by varying initial pH values in the range of 2.0–12.0. According to the results shown in Fig. 8, it is obvious that pH values affect the adsorption significantly. The amount of phosphate increased to 41.9 mg/g at pH of 3.0, and maintained this relatively high level between pH 3.0 and 7.0. While the phosphate deceased from 24.8 mg/g to 4.7 mg/g between pH 10 and 12. Phosphate acid can yield different species at different pHs as Eq. (6) show:

$$H_3PO_4 \overset{K_1}{\longleftrightarrow} H_2PO_4^{2-} + H^+ \overset{K_2}{\longleftrightarrow} HPO_4^- + 2H^+ \overset{K_3}{\longleftrightarrow} PO_4^{3-} + 3H^+ \quad (6)$$

where $pK_1 = 2.15$, $pK_2 = 7.20$ and $pK_3 = 12.33$, respectively.

At pH ≤ 2.13, the predominant species of phosphate is H_3PO_4 which is weakly attached to the sites of the adsorbent. When 2.13 < pH < 7.20, the main phosphate species presented as monovalent $H_2PO_4^-$ and the La-NN-M41 kept at a relatively high level between pH 3.0 and 7.0, which indicates that the lanthanum ions had greater affinity for the monovalent dihydrogen phosphate. This can be explained according to the hydroxylation of the lanthanum ions. The only insoluble $La(OH)_3$ forming at pH 7.58 undergoes the hydroxylation process in three steps. When pH is in the range of 3.0–7.0, the most likely form of lanthanum is $La(OH)_2^+$, which could match $H_2PO_4^-$• species at the stoichiometric ration of 1:1. However, this does not mean that the $H_2PO_4^{2-}$ is not adsorbed [40]. With the increase of pH, the lanthanum is mainly in its insoluble form $La(OH)_3$ which can hardly form $La(PO_4)_3$. The ion exchange mechanism may be predominant at high pH.

3.7. Effect of coexist anions on phosphate adsorption

The effects of added competitive anions F^-, Cl^-, NO_3^- and SO_4^{2-} are presented in Fig. 9. All the four group tests showed that the phosphate adsorption capacity decreased with the increase of competitive anions. The competitive anions' effects on phosphate adsorption follow the order: $SO_4^{2-} > F^- > Cl^- \approx NO_3^-$. There are many similar results reported by previous researchers, such as for $ZnCl_2$ activated coir pith carbon [43]: $ClO_4^- = SeO_3^{2-} > SO_4^{2-} > MoO_4^{2-} = VO_3^- = Cl^- = NO_3^-$, for calcined layered double hydroxides [8]: $SeO_3^{2-} > SO_4^{2-} > Cl^- > NO_3^-$. Among the four anions, SO_4^- has the strongest effect on the adsorption of phosphate on La-NN-M41. When the concentration of SO_4^- increased from 0 to 900 mg/L, the phosphate adsorption capacity of La-NN-M41 reduced from 42.2 mg/g to 19.5 mg/g. The decreases in the adsorption capacity may be explained on the basis of ion exchange mechanisms. The process of phosphate adsorption on the adsorbent occurs between phosphate ions and the hydroxide ions located on the adsorbent surface, and the gradually increased concentration of SO_4^{2-} will displace the PO_4^{2-} adsorbed on adsorbent. The affinity of adsorbents with competing ions determines the orders of the effect of anions on phosphate adsorption on La-NN-M41.

3.8. Desorption study

The preparation, phosphate adsorption, and desorption of La-NN-M41 are schematically illustrated in Fig. 10. The phosphate interacts with La^{3+} by electrostatic force and the interactions between phosphate and La^{3+} may be ionic. 0.01 M NaOH was used to treat the spent adsorbents. The desorption kinetics corresponding to spent adsorbents is shown in Fig. 11. It is clear that desorption

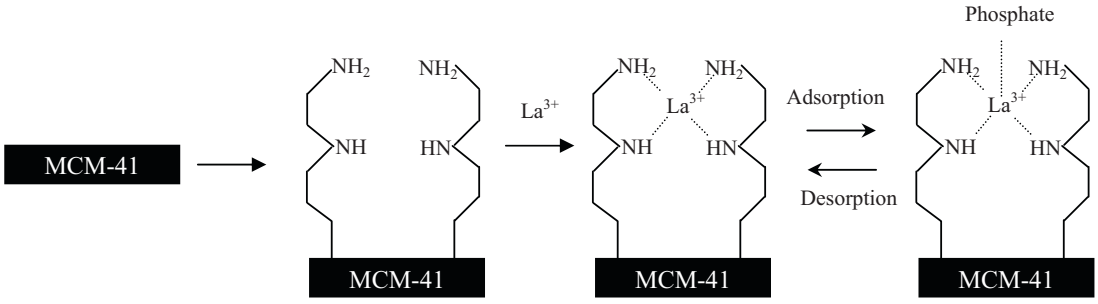

Fig. 10. The schematic drawing of the preparation, adsorption, desorption of La-NN-M41.

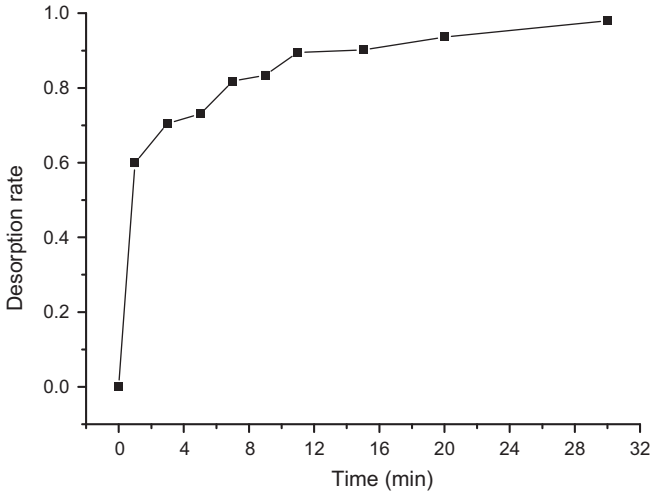

Fig. 11. Desorption kinetics of phosphate at 25 °C in 0.01 M NaOH solution.

is quick and almost completes within 12 min, which denotes that the adsorption of anions on La-NN-M41 is reversible.

4. Conclusions

Transition metal La immobilized onto the surface of diamino-functionalized MCM-41 was synthesized. The surface and structure property were conducted by XRD, pore size distribution, FTIR, and elemental analysis. In batch adsorption studies, the La-NN-M41 exhibits rapid adsorption rate and high adsorption capacity. The capacity increases with the increase in adsorbent loadings. The optimal pH for phosphate adsorption is between 3.0 and 7.0. The desorption rate is rapid and occurs within 12 min by using 0.01 M NaOH.

Acknowledgments

The authors acknowledge the financial support of the National Major Research Plan for Water Pollution Control and Treatment of China (2009ZX07101-015) and (2009ZX07105-003) for this study.

References

[1] E. Oguz, A. Gurses, M. Yalcin, Removal of phosphate from waste waters by adsorption, Water Air Soil Pollut. 148 (2003) 279–287.
[2] N.I. Chubar, V.A. Kanibolotskyy, V.V. Strelko, G.G. Gallios, V.F. Samanidou, T.O. Shaposhnikova, V.G. Milgrandt, I.Z. Zhuravlev, Adsorption of phosphate ions on novel inorganic ion exchangers, Colloid Surf. A 255 (2005) 55–63.
[3] S. Pitois, M.H. Jackson, B.J.B. Wood, Problems associated with the presence of cyanobacteria in recreational and drinking waters, Int. J. Environ. Health Res. 10 (2000) 203–218.
[4] P.P. Shen, Q. Shi, Z.C. Hua, F.X. Kong, Z.G. Wang, S.X. Zhuang, D.C. Chen, Analysis of microcystins in cyanobacteria blooms and surface water samples from Meiliang Bay, Taihu Lake, China, Environ. Int. 29 (2003) 641–647.
[5] Y.X. Xie, Z.Q. Xiong, G.X. Xing, X.Y. Yan, S.L. Shi, G.Q. Sun, Z.L. Zhu, Source of nitrogen in wet deposition to a rice agroecosystem at Tai lake region, Atmos. Environ. 42 (2008) 5182–5192.
[6] D.A. Georgantas, H.P. Grigoropoulou, Orthophosphate and metaphosphate ion removal from aqueous solution using alum and aluminum hydroxide, J. Colloid Interf. Sci. 315 (2007) 70–79.
[7] P. Papadopoulos, A. Dimirkou, A. Ioannou, Kinetics of phosphorus sorption by goethite and kaolinite–goethite (k–g) system, Commun. Soil Sci. Plan. 29 (1998) 2191–2206.
[8] J. Das, B.S. Patra, N. Baliarsingh, K.M. Parida, Adsorption of phosphate by layered double hydroxides in aqueous solutions, Appl. Clay Sci. 32 (2006) 252–260.
[9] U. Berg, A. Ehbrecht, E. Rohm, P.G. Weidler, R. Nuesch, Impact of calcite on phosphorus removal and recovery from wastewater using CSH-filled fixed bed filters, J. Residuals Sci. Technol. 4 (2007) 73–81.
[10] M.S. Onyango, D. Kuchar, M. Kubota, H. Matsuda, Adsorptive removal of phosphate ions from aqueous solution using synthetic zeolite, Ind. Eng. Chem. Res. 46 (2007) 894–900.
[11] S. Karaca, A. Gurses, M. Ejder, M. Acikyildiz, Kinetic modeling of liquid-phase adsorption of phosphate on dolomite, J. Colloids Interf. Sci. 277 (2004) 257–263.
[12] J. Pradhan, J. Das, S. Das, R.S. Thakur, Adsorption of phosphate from aqueous solution using activated red mud, J. Colloids Interf. Sci. 204 (1998) 169–172.
[13] A. Ugurlu, B. Salman, Phosphorus removal by fly ash, Environ. Int. 24 (1998) 911–918.
[14] B. Kostura, H. Kulveitova, J. Lesko, Blast furnace slags as sorbents of phosphate from water solutions, Water Res. 39 (2005) 1795–1802.
[15] X.P. Liao, Y. Ding, B. Wang, B. Shi, Adsorption behavior of phosphate on metal-ions-loaded collagen fiber, Ind. Eng. Chem. Res. 45 (2006) 3896–3901.
[16] C. Namasivayam, A. Sakoda, M. Suzuki, Removal of phosphate by adsorption onto oyster shell powder–kinetic studies, J. Chem. Technol. Biot. 80 (2005) 356–358.
[17] E.W. Shin, K.G. Karthikeyan, M.A. Tshabalala, Orthophosphate sorption onto lanthanum-treated lignocellulosic sorbents, Environ. Sci. Technol. 39 (2005) 6273–6279.
[18] T.L. Eberhardt, S.H. Min, Biosorbents prepared from wood particles treated with anionic polymer and iron salt: effect of particle size on phosphate adsorption, Bioresour. Technol. 99 (2008) 626–630.
[19] T.S. Anirudhan, B.F. Noeline, D.M. Mancihar, Phosphate removal from wastewaters using a weak anion exchanger prepared from a lignocellulosic residue, Environ. Sci. Technol. 40 (2006) 2740–2745.
[20] B.K. Biswas, K. Inoue, K.N. Ghimire, S. Ohta, H. Harada, K. Ohto, H. Kawakita, The adsorption of phosphate from an aquatic environment using metal-loaded orange waste, J. Colloids Interf Sci. 312 (2007) 214–223.
[21] R. Saad, K. Belkacemi, S. Hamoudi, Adsorption of phosphate and nitrate anions on ammonium-functionalized MCM-48: effects of experimental conditions, J. Colloids Interf. Sci. 311 (2007) 375–381.
[22] S. Hamoudi, R. Saad, K. Belkacemi, Adsorptive removal of phosphate and nitrate anions from aqueous solutions using ammonium-functionalized mesoporous silica, Ind. Eng. Chem. Res. 46 (2007) 8806–8812.
[23] L.W. Xu, M.S. Yang, J.X. Jiang, H.Y. Qiu, G.Q. Lai, Ionic liquid-functionalized SBA-15 mesoporous material: efficient heterogeneous catalyst in versatile organic reactions, Cent. Eur. J. Chem. 5 (2007) 1073–1083.
[24] T. Takei, O. Houshito, Y. Yonesaki, N. Kumada, N. Kinomura, Porous properties of silylated mesoporous silica and its hydrogen adsorption, J. Solid State Chem. 180 (2007) 1180–1187.
[25] V.J. Mayani, S.H.R. Abdi, R.I. Kureshy, N.H. Khan, S. Agrawal, R.V. Jasra, Synthesis and characterization of mesoporous silica modified with chiral auxiliaries for their potential application as chiral stationary phase, J. Chromatogr. A 1191 (2008) 223–230.
[26] F. Marlow, Optical materials based on nanoscaled guest/host composites, Mol. Cryst. Liq. Cryst. 341 (2000) 1093–1098.
[27] C.T. Kresge, M.E. Leonowicz, W.J. Roth, J.C. Vartuli, J.S. Beck, Ordered mesoporous molecular sieves synthesized by a liquid-crystal template mechanism, Nature 359 (1992) 710–712.
[28] X.S. Zhao, G.Q. Lu, A.K. Whittaker, G.J. Millar, H.Y. Zhu, Comprehensive study of surface chemistry of MCM-41 using Si-29 CP/MAS NMR, FTIR, pyridine-TPD, and TGA, J. Phys. Chem. B 101 (1997) 6525–6531.
[29] G.E Fryxell, J. Liu, T.A. Hauser, Z.M. Nie, K.F. Ferris, S. Mattigod, M.L. Gong, R.T. Hallen, Design and synthesis of selective mesoporous anion traps, Chem. Mater. 11 (1999) 2148–2154.
[30] R.S.S. Wu, K.H. Lam, J.M.N. Lee, T.C. Lau, Removal of phosphate from water by a highly selective La(III)-chelex resin, Chemosphere 69 (2007) 289–294.
[31] H.T. Zhao, K.L. Nagy, J.S. Waples, G.F. Vance, Surfactant-templated mesoporous silicate materials as sorbents for organic pollutants in water, Environ. Sci. Technol. 34 (2000) 4822–4827.
[32] T. Yokoi, H. Yoshitake, T. Tatsumi, Synthesis of amino-functionalized MCM-41 via direct co-condensation and post-synthesis grafting methods using mono-, di- and tri-amino-organoalkoxysilanes, J. Mater. Chem. 14 (2004) 951–957.
[33] American Public Health Association, Standard Methods for the Examination of Water and Wastewater, 16th ed., American Public Health Association, Washington, DC, 1985.
[34] M. Jang, J.K. Park, E.W. Shin, Lanthanum functionalized highly ordered mesoporous media: implications of arsenate removal, Micropor. Mesopor. Mater. 75 (2004) 159–168.
[35] S. Shylesh, A.P. Singh, Synthesis, characterization, and catalytic activity of vanadium-incorporated, -grafted, and -immobilized mesoporous MCM-41 in the oxidation of aromatics, J. Catal. 228 (2004) 333–346.
[36] S.M Rivera-Jimenez, A.J. Hernandez-Maldonado, Nickel(II) grafted MCM-41: a novel sorbent for the removal of Naproxen from water, Micropor. Mesopor. Mater. 116 (2008) 246–252.
[37] M. Kruk, M. Jaroniec, A. Sayari, Adsorption study of surface and structural properties of MCM-41 materials of different pore sizes, J. Phys. Chem. B 101 (1997) 583–589.
[38] R. Saad, S. Hamoudi, K. Belkacemi, Adsorption of phosphate and nitrate anions on ammonium-functionalized mesoporous silicas, J. Porous Mater. 15 (2008) 315–323.
[39] H. Li, J.Y. Ru, W. Yin, X.H. Liu, J.Q. Wang, W.D. Zhang, Removal of phosphate from polluted water by lanthanum doped vesuvianite, J. Hazard. Mater. 168 (2009) 326–330.
[40] F. Haghseresht, S.B. Wang, D.D. Do, A novel lanthanum-modified bentonite, Phoslock, for phosphate removal from wastewaters, Appl. Clay Sci. 46 (2009) 369–375.
[41] S. Lagergren, Zur theorie der sogenannten adsorption gelöster stoffe, Kungliga Svenska Vetenskapsakademiens, Handlingar 24 (1898) 1–39.

[42] G. Blanchard, M. Maunaye, G. Martin, Removal of heavy metals from waters by means of natural zeolites, Water Res. 18 (1984) 1501–1507.
[43] C. Namasivayam, D. Sangeetha, Equilibrium and kinetic studies of adsorption of phosphate onto $ZnCl_2$ activated coir pith carbon, J. Colloids Interf. Sci. 280 (2004) 359–365.
[44] N. Ping, H.J. Bart, L. Bing, X.W. Lu, Y. Zhang, Phosphate removal from wastewater by model-La(III) zeolite adsorbents, J. Environ. Sci.-China 20 (2008) 670–674.
[45] E.W. Shin, J.S. Han, M. Jang, S.H. Min, J.K. Park, R.M. Rowell, Phosphate adsorption on aluminum-impregnated mesoporous silicates: surface structure and behavior of adsorbents, Environ. Sci. Technol. 38 (2004) 912–917.
[46] G.S. Zhang, H.J. Liu, R.P. Liu, J.H. Qu, Removal of phosphate from water by a Fe-Mn binary oxide adsorbent, J. Colloids Interf. Sci. 335 (2009) 168–174.
[47] H.L. Liu, X.F. Sun, C.G. Yin, C. Hu, Removal of phosphate by mesoporous ZrO_2, J. Hazard. Mater. 151 (2008) 616–622.